JACS
JOURNAL OF THE AMERICAN CHEMICAL SOCIETY

ARTICLE

pubs.acs.org/JACS

Bithiophene-Imide-Based Polymeric Semiconductors for Field-Effect Transistors: Synthesis, Structure−Property Correlations, Charge Carrier Polarity, and Device Stability

Xugang Guo,[†] Rocio Ponce Ortiz,[†] Yan Zheng,[‡] Yan Hu,[‡] Yong-Young Noh,[§] Kang-Jun Baeg,[∥] Antonio Facchetti,[*,†,‡] and Tobin J. Marks[*,†]

[†]Department of Chemistry and the Materials Research Center, Northwestern University, 2145 Sheridan Road, Evanston, Illinois 60208, United States

[‡]Polyera Corporation, 8045 Lamon Avenue, Skokie, Illinois 60077, United States

[§]Department of Chemical Engineering, Hanbat National University, 16-1 Dukmyung-dong, Yuseong-gu, Daejeon, 305-719, Republic of Korea

[∥]Convergence Components & Materials Laboratory, Electronics and Telecommunications Research Institute (ETRI), 138 Gajeongno, Yuseong-gu, Daejeon 305-350, Republic of Korea

Supporting Information

ABSTRACT: Developing new high-mobility polymeric semiconductors with good processability and excellent device environmental stability is essential for organic electronics. We report the synthesis, characterization, manipulation of charge carrier polarity, and device air stability of a new series of bithiophene-imide (BTI)-based polymers for organic field-effect transistors (OFETs). By increasing the conjugation length of the donor comonomer unit from monothiophene (**P1**) to bithiophene (**P2**) to tetrathiophene (**P3**), the electron transport capacity decreases while the hole transport capacity increases. Compared to the BTI homopolymer **P(BTimR)** having an electron mobility of 10^{-2} cm^2 V^{-1} s^{-1}, copolymer **P1** is ambipolar with balanced hole and electron mobilities of $\sim 10^{-4}$ cm^2 V^{-1} s^{-1}, while **P2** and **P3** exhibit hole mobilities of $\sim 10^{-3}$ and $\sim 10^{-2}$ cm^2 V^{-1} s^{-1}, respectively. The influence of **P(BTimR)** homopolymer M_n on film morphology and device performance was also investigated. The high M_n batch **P(BTimR)-H** affords more crystalline film microstructures; hence, 3× increased electron mobility (0.038 cm^2 V^{-1} s^{-1}) over the low M_n one **P(BTimR)-L** (0.011 cm^2 V^{-1} s^{-1}). In a top-gate/bottom-contact OFET architecture, **P(BTimR)-H** achieves a high electron mobility of 0.14 cm^2 V^{-1} s^{-1}, only slightly lower than that of state-of-the-art n-type polymer semiconductors. However, the high-lying **P(BTimR)-H** LUMO results in minimal electron transport on exposure to ambient. Copolymer **P3** exhibits a hole mobility approaching 0.1 cm^2 V^{-1} s^{-1} in top-gate OFETs, comparable to or slightly lower than current state-of-the-art p-type polymer semiconductors (0.1−0.6 cm^2 V^{-1} s^{-1}). Although BTI building block incorporation does not enable air-stable n-type OFET performance for **P(BTimR)** or **P1**, it significantly increases the OFET air stability for p-type **P2** and **P3**. Bottom-gate/top-contact and top-gate/bottom-contact **P2** and **P3** OFETs exhibit excellent stability in the ambient. Thus, **P2** and **P3** OFET hole mobilities are almost unchanged after 200 days under ambient, which is attributed to their low-lying HOMOs (>0.2 eV lower than that of **P3HT**), induced by the strong BTI electron-withdrawing capacity. Complementary inverters were fabricated by inkjet patterning of **P(BTimR)-H** (n-type) and **P3b** (p-type).

INTRODUCTION

Solution-processable organic semiconductors are attractive for their potential applicability in low-cost electronics and compatibility with plastic substrates, thereby enabling mechanically flexible circuits.[1−4] Major applications of organic semiconductor-based electronics include organic light-emitting diodes (OLEDs),[5,6] organic field-effect transistors (OFETs),[7,8] organic photovoltaic (OPV) cells,[9,10] and organic electrochromic devices (ECDs).[11,12] The key attraction of organic semiconductors versus conventional inorganic-based materials is the possibility of fabricating electronic devices by solution-based methodologies such as spin coating and printing.[13−16] Thus, the pivotal prerequisite to advance from emerging prototypes to widespread applications is to develop high-performance soluble organic semiconductors with acceptable performance and robust air stability.[17]

After extensive research efforts by industry, government, and academia, several high-performance organic semiconductor classes have emerged.[18] With few exceptions, organic semiconducting materials can be divided into two classes: small molecules (or oligomers)[19,20] and macromolecules,[21] both offering distinct advantages and disadvantages in terms of processability and device performance.[2,22] Organic small molecules having well-defined chemical structures can be obtained in high purity levels through conventional purification techniques such as chromatography, sublimation, and recrystallization. Both vacuum evaporation and solution-based techniques can be employed to fabricate OFETs using small molecule films as the active component.[19] Using

Received: August 30, 2010
Published: January 5, 2011

dx.doi.org/10.1021/ja107678m | *J. Am. Chem. Soc.* 2011, 133, 1405–1418

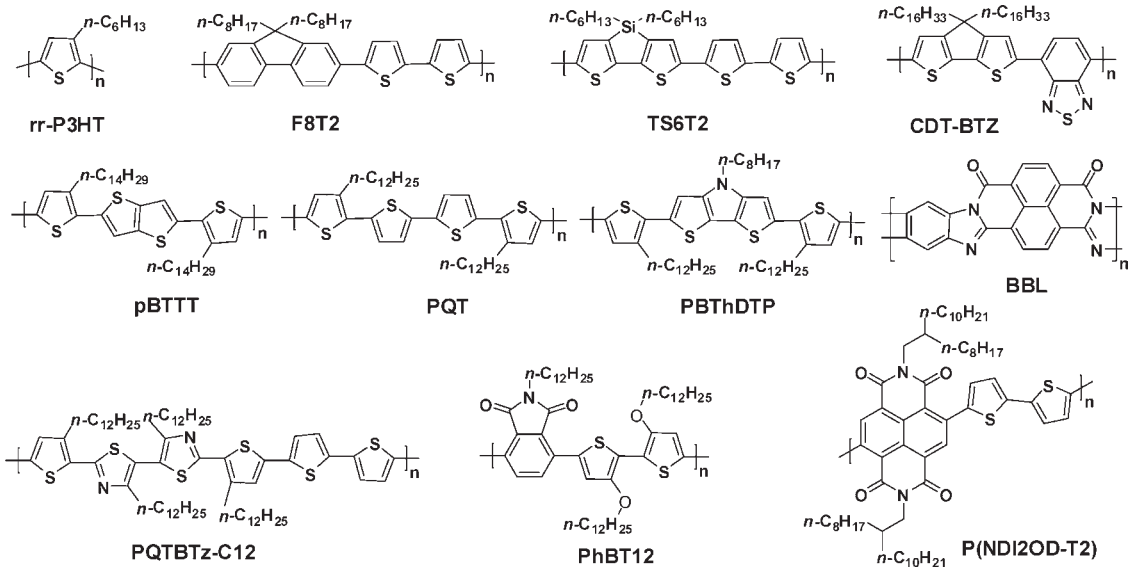

Figure 1. Structures of representative polymeric semiconductors for high-performance OFETs.

solution-based film growth techniques, substantial carrier mobilities (up to 1.0 $cm^2\ V^{-1}\ s^{-1}$)[23] can be obtained with small molecules due to their highly ordered film microstructures.[24] Nevertheless, small molecule semiconductors generally lack good solution film-forming properties due to the limited achievable solution viscosities, presenting a challenge to widespread applications in printed electronics.[18] In contrast, polymers are polydisperse materials systems for which large-scale purification methods are generally limited to reprecipitation or extraction (e.g., Soxhlet). Trace impurities that are difficult to remove from polymers may significantly compromise device performance. Furthermore, OFET performance reproducibility from polymer batch to batch can be problematic due to molecular weight and polydispersity variations.[25−27] Thus, dispersion in the polymer chain length may adversely affect self-organization during film formation, resulting in lower OFET carrier mobility in comparison to small molecules.[2] However, polymeric semiconductors typically exhibit minimal grain boundaries and excellent film-forming properties, which are essential for fabrication of large-area devices by printing.[18]

In the evolution of high-performance polymer semiconductors (Figure 1), the development of highly regioregular poly(3-hexylthiophene) (**rr-P3HT** or **P3HT**) marked a milestone in the OFET field.[28,29] A hole mobility greater than 0.1 $cm^2\ V^{-1}\ s^{-1}$ was achieved by optimizing film microstructure and device design.[30−33] Understanding the relationship between charge transport and film microstructure provided chemists with fundamental design rules for designing optimum OFET materials.[17,21,34] In contrast to regioregular poly(3-hexylthiophene), regioirregular (or regiorandom) poly(3-hexylthiophene) (**ri-P3HT**) exhibits several orders of magnitude lower mobility[21] and head-to-head (HH) linkages in **ri-P3HT** induce steric repulsion between neighboring thiophene units, resulting in a twisted polymer backbone which eliminates three-dimensional structural ordering in the solid state.

To maintain good processability and to avoid HH linkage-induced steric repulsion, two common approaches have been utilized in designing new materials. In the first, a bridging atom is used to lock the conformation between adjacent aromatic rings, thus enforcing a coplanar polymer backbone. This strategy yields large charge carrier mobilities for **F8T2**,[35] **TS6T2**,[36] and **CDT-BTZ**[37] (Figure 1). The second widely used approach is to insert a spacer between alkylated bithiophene units, as reported for **pBTTT**,[38] **PQT**,[39] and **PBThDTP** (Figure 1).[40] These regiosymmetric polythiophenes exhibit excellent device performance with hole mobilities as high as 0.6 $cm^2\ V^{-1}\ s^{-1}$ (**pBTTT**).[17,21] Recently, Bao[41] and Watson[42] reported the high-mobility p-type polymeric semiconductors **PQTBTz-C12**[41] and **PhBT12**[42] with HH linkages in the polymer backbones and having hole mobilities up to 0.3 $cm^2\ V^{-1}\ s^{-1}$. The high mobilities are due to well-organized solid state nanostructures, enabled by intermolecular $\pi-\pi$ interactions in **PQTBTz-12**[43] and by close intramolecular sulfur−oxygen contacts in **PhBT12**.[44,45]

Although current state-of-the-art polymer semiconductors exhibit hole[21] and electron mobilities comparable to that of amorphous silicon (a-Si) (**BBL**[46] and **P(NDI2OD-T2)**[14] in Figure 1),[14,31,46] their technological application is hindered by poor air stability.[17] P-doping by reaction with ambient O_2 and ozone results in decreased hole mobilities,[38,47] increased off currents, and hence lower I_{on}/I_{off} ratios as well as a positive shift of the threshold voltage.[48,49] For π-electron organic semiconductors, the frontier molecular orbital (FMO) energies play a crucial role in device stability.[15] For n-type organic semiconductors, the electron affinity (EA) controls the resistance of conducting organic radical anions to oxidative dopants such as O_2, H_2O, and ozone.[50] Lowering the energy of the lowest unoccupied molecular orbitals (LUMOs) has been shown to enhance the air stability of n-type materials.[51−53] For p-type organic semiconductors, a relatively low ionization potential (IP) will result in p-type doping, and thus, lowering the energies of the highest occupied molecular orbitals (HOMOs) results in increased air stability.[54] Therefore, fine tuning of the semiconductor FMO energies must be a major focus for improving OFET stability.[55,56] Diverse strategies have been used to enhance the device stability. For example, **pBTTT** exhibits superior air stability versus **P3HT** because the thienothiophene ring has greater resonance stabilization than thiophene, resulting in enhanced localization and a HOMO lowered by ~0.1 eV.[17] Also, the fluorene unit has been inserted into the polythiophene backbone of **F8T2** to enhance stability.[36] A donor−acceptor strategy is another effective

dx.doi.org/10.1021/ja107678m |*J. Am. Chem. Soc.* 2011, 133, 1405–1418

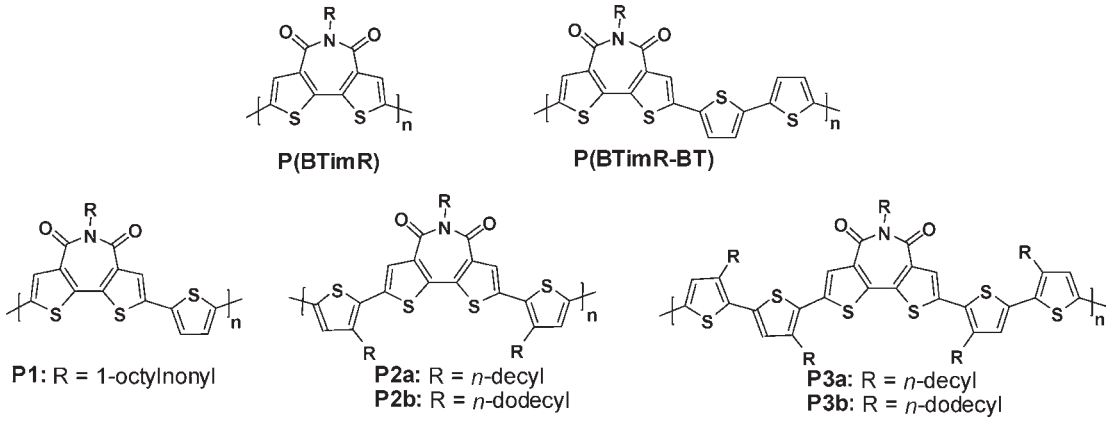

Figure 2. Structures of BTI-based homopolymers and copolymers for OFETs, where **P(BTimR)** and **P(BTimR-BT)** have been reported by us previously.[60]

approach,[48,57] and thus, silole-based polymer **TS6T2** (Figure 1) has a significantly lower HOMO energy (−5.2 eV) than that of **P3HT** (−4.9 eV), a demonstrated mobility approaching 0.06 $cm^2 V^{-1} s^{-1}$, and undergoes negligible degradation of OFET characteristics after 2000 repeated on−off cycles under ambient conditions.[36] Although several polymeric semiconductors with low HOMO energies have been synthesized, these materials usually exhibit low hole mobilities (<0.01 $cm^2 V^{-1} s^{-1}$) due to the energetic barrier for hole injection from the Fermi level of the Au electrode.[35,58,59] Thus, developing materials with low-lying HOMOs to enhance air stability and yet enable high carrier mobility remains an important scientific challenge.[17]

We report here a new series of bithiophene-imide (BTI)-based conjugated copolymers for OFETs created by sequentially varying the conjugation length of the electron-donor block. Our previous work demonstrated that the BTI building block is highly planar and exhibits antiparallel BTI packing and close $\pi-\pi$ stacking in the solid state, and that polymers constructed from BTI units can exhibit high solubility in common organic solvents.[60] The BTI-based homopolymers **P(BTimR)** (Figure 2) are highly crystalline and exhibit moderate electron mobility (0.011 $cm^2 V^{-1} s^{-1}$), while BTI-based copolymers **P(BTimR-BT)** exhibit a hole mobility of 0.008 $cm^2 V^{-1} s^{-1}$, despite the low molecular weight (M_n = 1.8 KDa) and poor solubility. Here we first investigate how the **P(BTimR)** homopolymer molecular weight affects FET performance by synthesizing high (**P(BTimR)-H**) and low (**P(BTimR)-L**) molecular weight batches. The high molecular weight batch affords an electron mobility of ∼0.04 $cm^2 V^{-1} s^{-1}$ in bottom-gate OFETs, which is 3× larger than the mobility we previously reported for **P(BTimR)** (here **P(BTimR)-L**). The mobility of **P(BTimR)-H** measured in top-gate OFETs is up to 0.19 $cm^2 V^{-1} s^{-1}$, which is slightly lower than that of **P(NDI2OD)-T2**.[14] However, the high LUMO energy of the homopolymer prevents electron transport when the devices are exposed to air. We next further develop BTI-based polymer architectures by copolymerization with selected electron-donating oligothiophenes (**P1**−**P3**, Figure 2). It will be seen that using the monothiophene unit as a donor yields copolymer **P1** which exhibits ambipolar behavior having balanced hole and electron mobilities (4×10^{-4} $cm^2 V^{-1} s^{-1}$). Using a TT linkage containing bithiophene as a donor yields copolymers **P2** which exhibit a moderate hole mobility of 2×10^{-3} $cm^2 V^{-1} s^{-1}$. Using tetrathiophene as a donor affords copolymers **P3**, which exhibit substantial solubility and crystallinity and in top-gate/bottom-contact OFETs, and have a hole mobility approaching 0.1 $cm^2 V^{-1} s^{-1}$, similar to the performance of **P3HT** OFETs fabricated under the same conditions.[14] Furthermore, due to the low HOMO energies of **P2** and **P3**, OFETs fabricated from them exhibit enhanced device air stability. Among them, both bottom-gate/top-contact (BG/TC) and top-gate/bottom-contact (TG/BC) devices fabricated from **P3** exhibit negligible performance degradation (mobility, I_{on}/I_{off} ratio, V_t) after exposure to ambient for 9 months. We believe that these new polymers offer significant attractions versus other state-of-the-art p-type polymer semiconductors which degrade faster[40,47] or in which enhanced air stability is achieved by controlling atmospheric humidity.[38,61,62] The present results show that BTI is effective in tuning FMO energies and that proper self-assembly of these polymers achieves both high mobility (∼0.1 $cm^2 V^{-1} s^{-1}$) and ambient stability.

RESULTS AND DISCUSSION

The materials design strategy in this study grows out of previous research using BTI as a novel building block for constructing polymeric semiconductors.[60] However, the n-type BTI homopolymer **P(BTimR)** suffers from poor OFET air stability, and the p-type bithiophene-containing BTI copolymer **P(BTimR-BT)** has limited solubility and low mobility. Using monothiophene or alkylated oligothiophenes as donor units, we show here that the present approach affords BTI-based copolymers having higher molecular weights and greater solubilities than **P(BTimR-BT)**. Furthermore, dilution of the BTI loading in the polymer backbones results in polymers with tunable FMO energies, increased hole mobilities, and far greater p-type OFET environmental air stability.

The materials presented here are characterized by NMR, EA, GPC, DSC, optical spectroscopy, and electrochemistry. XRD and AFM are employed to characterize and analyze the microstructure and morphology of the spin-cast films, followed by FET device fabrication, evaluation, and optimization. Then device air stability over time is evaluated and discussed as a function of macromolecular architecture and electronic structure. Finally, functional complementary inverters are fabricated from these materials by inkjet printing.

Synthesis of Monomers and Polymers. The synthesis of the BTI-based monomers and polymers is depicted in Schemes 1

Scheme 1. Synthetic Routes to Comonomers for BTI Polymer Synthesis[a]

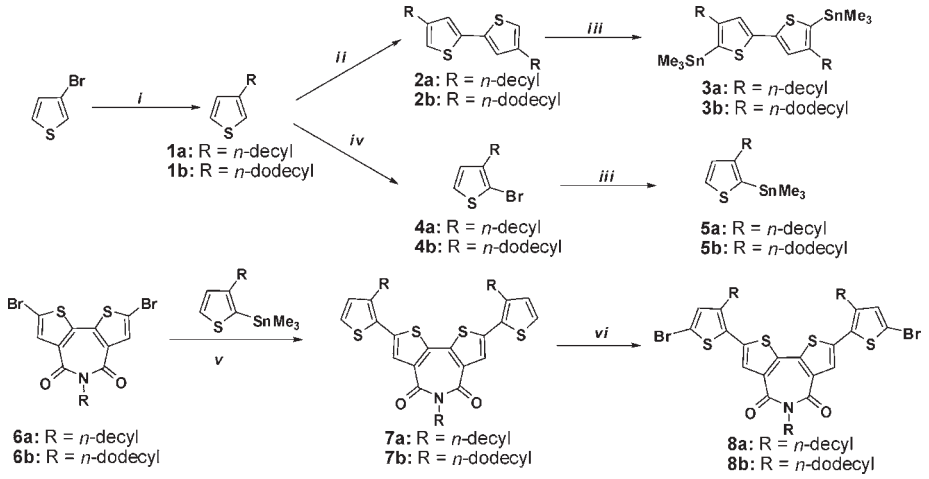

[a] Reagents and conditions: (*i*) *n*-RMgBr, Ni(dppp)Cl_2, ether, 12 h, 60 °C; (*ii*) *n*-BuLi, TMEDA, $CuCl_2$, ether, reflux to −78 °C, then to rt; (*iii*) *n*-BuLi, Me_3SnCl, THF, −78 °C to rt; (*iv*) NBS, $CHCl_3$/HOAc, rt, 2 h; (*v*) $PdCl_2(PPh_3)_2$, THF, 90 °C, 12 h; (*vi*) Br_2, $CHCl_3$/HOAc, rt, 4 h.

Scheme 2. Synthesis of BTI-Based Copolymers[a]

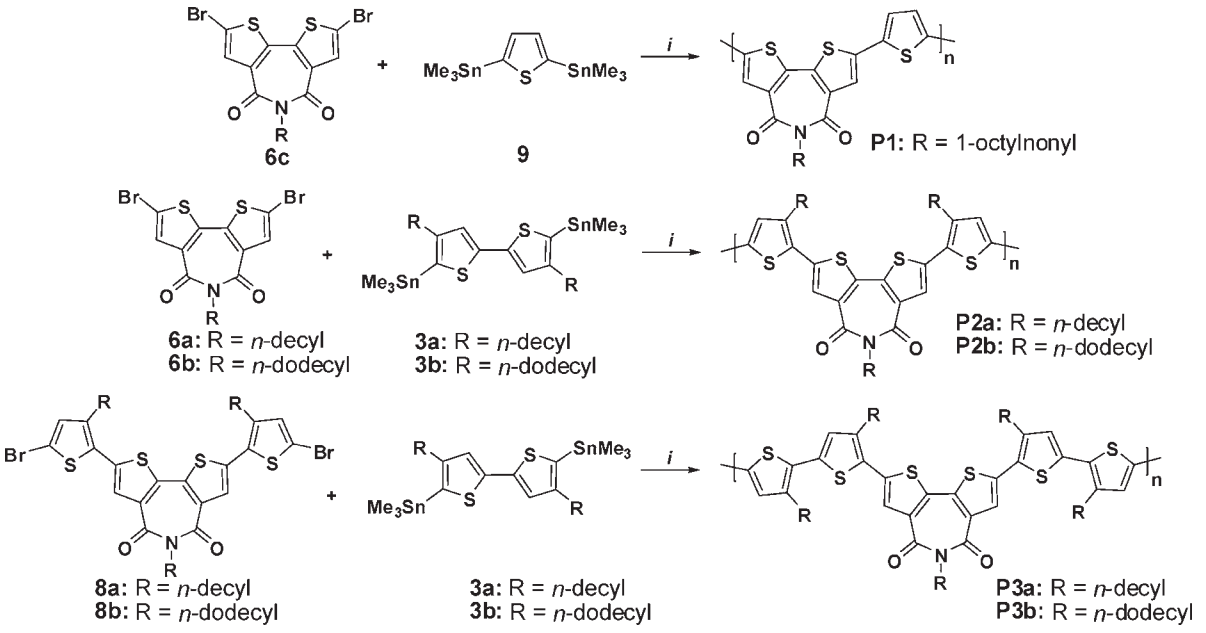

[a] Reagents and conditions: (*i*) $Pd_2(dba)_3$, P(*o*-tolyl)$_3$, THF, 80 °C.

and 2. To increase the solubility of the BTI-based polymers and at the same time to retain close $\pi-\pi$ stacking, tail-to-tail (TT) linkages containing bithiophene units **2a** and **2b**[52] were incorporated into the polymer backbones. The monomer precursors **2a** and **2b** were synthesized following published procedures.[63] The precursors were easily converted to monomers **3a** and **3b** by *n*-BuLi lithiation of **2a** and **2b**, respectively, and then quenching with trimethylstannyl chloride. ^1H and ^{13}C NMR spectroscopy indicates that the crude monomers are already quite pure (>90%), and purification of **3a** and **3b** is easily accomplished by recrystallization from hexane at −78 °C to afford the target products in high yields (>80%). The synthesis of key BTI building block **6** was first reported from this laboratory in 2008.[60] The synthesis of **8a** and **8b** starts from **6a** and **6b**, respectively, which were reacted with the corresponding 2-trimethylstannyl-3-alkylthiophenes **5a** and **5b** under Stille coupling conditions to afford monomer precursors **7a** and **7b** in moderate yields (>50%). Monomers **8a** and **8b** were then obtained in high yields (>90%) by reaction of **7a** and **7b** with bromine.

The syntheses of BTI-based polymers **P1**−**P3** (Scheme 2) were carried out using metal-catalyzed Stille polymerizations with $Pd_2(dba)_3$/P(*o*-tolyl)$_3$ as the catalyst in THF at 80 °C. The polymerization times were varied to optimize the solubility and processability of the product polymers. After polymerization was complete, 2-(tributylstannyl)thiophene was added and the reaction mixtures stirred for another 24 h to end cap the polymer chains. The reactions were then quenched in methanol and the product copolymers collected by filtration. Purifications were

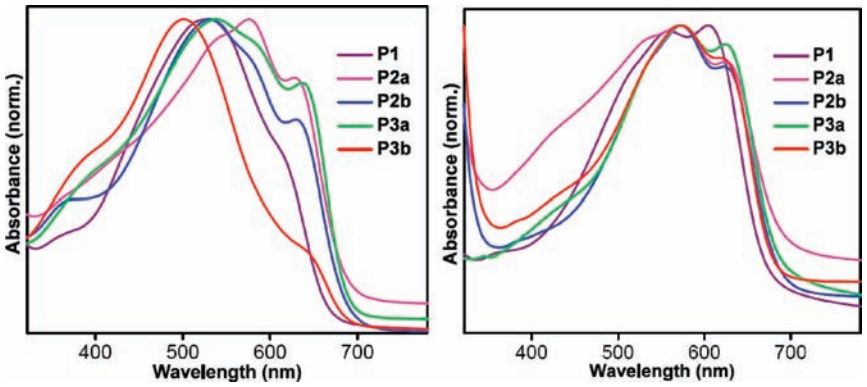

Figure 3. Optical absorption spectra of polymer **P1**−**P3** solutions (left) in chloroform (1×10^{-5} M) and as pristine films (right) cast from chlorobenzene (5 mg/mL).

accomplished by Soxhlet extraction using different solvent sequences, depending on the polymer solubility. Due to the low volume fraction of solubilizing alkyl chains in **P1**, "swallow-tail"-like branched side chains (1-octylnonyl) were used in this polymer, which then exhibits acceptable solubility in warm chlorinated solvents (>5 mg/mL). Note however that incorporation of linear chains or branched 2-octyldodecyl chains[60] results in insoluble or poorly soluble **P1** derivatives. **P2a** has a high volume fraction of solubilizing chains, and the major fraction can be extracted with hot chlorobenzene. While polymer **P2a** shows decent solubility in hot chlorobenzene, it is barely soluble at room temperature, which significantly affects the processability and film quality in the corresponding OFET devices (vide infra). The other polymers exhibit excellent solubility in chlorinated solvents. The fraction of **P3b** used for OFET fabrication can be extracted with hexane due to the large number of long alkyl substituents. The identity and purity of all polymers is supported by elemental analysis (EA) and high-temperature ^{1}H NMR spectra in 1,1,2,2-tetrachloroethane-d_2 (see Supporting Information for details). The EA demonstrates high purity with error lower than 0.5% for C, H, and N for all polymers except **P2a**. The EA of **P2a** gives 68.12% for C, 7.99% for H, 1.84% for N, and 3.60% for ash. The ash is due to the Pd residues from catalyst. Adjusting the numbers to an ash-free formulation gives 70.66% for C, 8.29% for H, and 1.91% for N, which is comparable to theoretical values. The reason for contaminating Pd in the **P2a** sample is likely due to the low solubility of **P2a** at room temperature, which prevents filtration of the **P2a** solution through a 0.22 μm PTFE filter used to remove the Pd particles. However, all other polymer solutions can be easily filtered through the filter before sending for elemental analysis. This could lead to the significant amount of Pd in the **P2a** sample but not in other samples.

In order to investigate the effect of **P(BTimR)** molecular weight on film morphology and device performance, different polymerization procedures and postpurification conditions were employed by varying reaction temperature, reaction solvent, and the solvent sequence of Soxhlet extractions. Thus, three batches of polymers with different molecular weight and processability were obtained (see Supporting Information): **P(BTimR)-L** (low molecular weight batch), **P(BTimR)-H** (high molecular weight batch), and **P(BTimR)-I** (insoluble batch). Among them, **P(BTimR)-L** was synthesized and purified under the exactly same conditions reported by some of us before.[60] Note also that two batches were synthesized for each of **P1**−**P3** under the same conditions and that comparable results were achieved (Supporting Information). The results show good reproducibility in the synthesis of these BTI-based polymers. The number-average molecular weight (M_n) and polydispersity (PDI) were 4.0 kDa and 2.12, respectively, for **P(BTimR)-L**, which is comparable to our previous result of M_n = 3.6 kDa and PDI = 2.20.[60] By increasing the polymerization temperature from 60 to 80 °C and recovering the polymer using chloroform as solvent after hexane extraction, **P(BTimR)-H** was obtained with M_n = 7.2 kDa and PDI = 1.98. However, polymerization in DMF and toluene as cosolvents at 80 °C results in insoluble **P(BTimR)-I**, which could not be further processed.

Polymer Optical Properties. The optical absorption spectra of polymers **P1**−**P3** in solution and as thin films are shown in Figure 3, and relevant data are summarized in Table 1. All polymers exhibit large oscillator strengths in the visible region ranging from λ_{max} = 502 to 576 nm in solution and from λ_{max} = 558 to 574 nm for the thin films. The corresponding optical band gaps are estimated from the red absorption edge and fall within a small range for all the present polymers, both in solution (1.80−1.81 eV) and in the solid state (1.81−1.85 eV). The band gaps of **P1**−**P3** are smaller than that of **rr-P3HT** (1.90−2.0 eV)[64,65] and the BTI homopolymer **P(BTimR)** (2.02 eV), which can be attributed to the donor−acceptor interactions in these BTI-based copolymers. Although the band gaps of the new polymers are within a small range, it is interesting to note that the E_g^{opt}s of **P2** and **P3** are slightly smaller than that of **P1** due to the stronger donating ability of the bithiophene donor units of **P2** and the tetrathiophene units of **P3** vs that of the monothiophene unit of **P1**. When considering polymers with the same backbone, those having shorter side chains have a stronger tendency to aggregate in solution. In chloroform, the λ_{max} of **P2b** is 45 nm blue-shifted in comparison to that of **P2a** and the λ_{max} of **P3b** is 37 nm blue-shifted vs that of **P3a**. However, note that the thin film absorption spectra are almost identical ($\Delta\lambda_{max}$ = 1 nm). On going from solution to the solid state, these polymers exhibit different bathochromic shifts which reflect different levels of backbone planarization and interchain $\pi-\pi$ interactions. Although **P(BTimR)-H** has a higher molecular weight than **P(BTimR)-L**, both batches show identical optical absorption profiles, indicating that saturation of the conjugation length is already present in **P(BTimR)-L**.

The thin films of the present polymer family exhibit both an absorption maximum and a shoulder at longer wavelength than in solution, similar to the vibronic profiles seen in regioregular polythiophene spectra.[29] This indicates highly ordered

Table 1. Optical and Electrochemical Properties of Polymers P1−P3 vs those of P3HT, P(BTimR), and P(BTimR-BT)

polymer	λ_{max} abs sol (nm)[a]	$\lambda_{shoulder}$ abs sol (nm)[a]	λ_{max} abs film (nm)[b]	$\lambda_{shoulder}$ abs film (nm)[b]	E_g^{opt} (eV)[c]	E_{ox}^{onset} (V)[d]	E_{HOMO} (eV)[e]	E_{red}^{onset} (V)[d]	E_{LUMO} (eV)[f]
P3HT	447	NA	551	603	1.90	0.33	−5.13	NA	NA (−3.23)
P(BTimR)[h]	535	578	524	564	2.02	1.48	−6.28	−1.33	−3.47
P(BTimR-BT)[h]	517	607	569	615	1.91	1.08	−5.88	−1.76	−3.04
P1	527	618	558	615	1.85	0.75	−5.55	−1.47	−3.33 (−3.70[g])
P2a	576	638	572	630	1.81	0.65	−5.45	−1.58	−3.22 (−3.64[g])
P2b	531	640	573	632	1.82	0.64	−5.44	−1.54	−3.26 (−3.63[g])
P3a	539	646	574	633	1.82	0.60	−5.40	NA	NA (−3.58[g])
P3b	502	649	573	632	1.83	0.58	−5.38	NA	NA(3.55[g])

[a] Solution absorption spectra (1×10^{-5} M in chloroform). [b] Thin film absorption spectra from pristine film cast from 5 mg/mL chlorobenzene solution. [c] Optical band gap estimated from the absorption edge of the as-cast thin film. [d] Electrochemically determined vs Fc/Fc^+. [e] $E_{HOMO} = -(E_{ox}^{onset} + 4.80)$. [f] $E_{LUMO} = -(E_{red}^{onset} + 4.80)$. [g] Values in parentheses calculated according to $E_{LUMO} = E_g^{opt} + E_{HOMO}$. [h] Data from ref 60 for **P(BTimR)** and **P(BTimR-BT)**, in which R = 2-octyldodecyl.

three-dimensional solid state structures.[48] Note that thermal annealing of the pristine films under N_2 at 150 °C does not alter the optical absorption profiles. It is worth comparing the absorption spectra and optical band gaps of the bithiophene-containing **P2** and **P(BTimR-BT)** polymers (structures shown in Figure 2). The band gap of **P2** is slightly smaller than that of **P(BTimR-BT)** (ΔE_g^{opt} = 0.1 eV, Table 1),[60] which implies that **P2** maintains the same backbone conformation as **P(BTimR-BT)** and has a greater number of repeat units due to the higher molecular weight afforded by the enhanced solubility of **P2** vs **P(BTimR-BT)** and the electron-releasing capacity of the alkyl chains on the bithiophene comonomer unit of **P2**.[17] Since the optical band gaps of all BTI copolymers and **P3HT** are similar, the electron-deficient imide group apparently lowers both the HOMO and the LUMO energies; this will be investigated by cyclic voltammetry in the next section. Lower HOMOs are generally predictors of greater air stability in OFETs.

Polymer Electrochemical Properties. It is known that organic semiconductors must have appropriate HOMO or LUMO energies to facilitate hole (p-type) or electron (n-type) injection from the source electrode and to optimize charge transport in the FET channel as well as device environmental stability.[51] The electrochemical properties of the BTI-based polymers were investigated as thin films in anhydrous acetonitrile under N_2 at a scan rate of 50 mV/s using tetrakis(*n*-butyl)ammonium hexafluorophosphate ($(n\text{-Bu})_4NPF_6$) as the supporting electrolyte. Platinum electrodes were used as both the working electrode and the counter electrode, and a Ag wire was used as the pseudoreference electrode. Polymer films were drop cast onto the platinum working electrode from a 0.2% (w/w) chlorobenzene solution. A ferrocene/ferrocium (Fc/Fc^+) redox couple was used as the internal standard and assigned an absolute energy of −4.80 eV vs vacuum.[66] The peaks of the Fc/Fc^+ redox couple are relatively poorly resolved in some traces, which could be due to the film thickness. The thick film may lead to inefficient penetration of electrolyte and ferrocene through the polymer films. The poor resolution of peaks can result in large experimental errors; thus, the data reported in Table 1 are estimated from at least two runs for each polymer sample to minimize the experimental errors. All

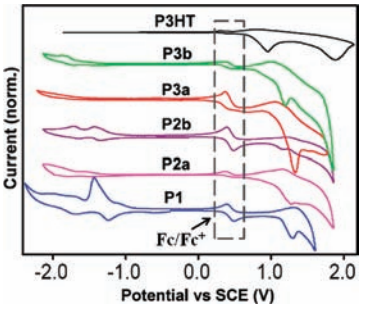

Figure 4. Cyclic voltammograms of BTI copolymer thin films (Fc/Fc^+ redox couple was used as internal standard). **P3HT** is shown for comparison.

electrochemical potentials are reported vs SCE (Figure 4), which has an energy of −4.44 eV below the vacuum level.[67] The HOMO energies of **P1**−**P3** were determined from the oxidation onset of the CV curves and calculated according to eq 1 (E_{ox}^{onset} = onset oxidation potential vs Fc/Fc^+).

$$E_{HOMO} = -(E_{ox}^{onset} + 4.80)(eV) \quad (1)$$

$$E_{LUMO} = -(E_{red}^{onset} + 4.80)(eV) \quad (2)$$

$$E_{LUMO} = E_g^{opt} + E_{HOMO}(eV) \quad (3)$$

All of the present BTI-based copolymers exhibit detectable quasi-reversible oxidation waves. The onset oxidation potentials (vs Fc/Fc^+) are +0.75, +0.65, +0.64, +0.60, and +0.58 V for **P1**, **P2a**, **P2b**, **P3a**, and **P3b**, respectively (Table 1). As expected, a change of alkyl substituent length has a negligible influence on the polymer electrochemical properties. However, increasing the conjugation length of the donor from monothiophene (**P1**) to bithiophene (**P2**) reduces the onset of the oxidation potential significantly by ∼0.1 V, and further increasing the donor conjugation length from bithiophene (**P2**) to tetrathiophene (**P3**) decreases the oxidation potential onset further by ∼0.05 V. The more facile oxidation on going from **P1** to **P3** is due to the increased electron-donating capacity of tetrathiophene vs monothiophene,

Table 2. Bottom-Gate/Top-Contact (BG/TC) OFET Performance for Polymers P1−P3, P3HT, P(BTimR), and P(BTimR-BT) Measured in Ambient Conditions

polymer	casting solvent	$T_{annealing}$ (°C)/time (h)	μ ($cm^2\ V^{-1}\ s^{-1}$)[c]	V_t (V)	I_{on}/I_{off}
P1[a]	DCB	150/2	3.6×10^{-4} ($\pm 2.2 \times 10^{-4}$) [h]	−95	5×10^3
			4.6×10^{-4} ($\pm 6.5 \times 10^{-5}$) [e]	100	10^4
P2a	CB	150/2	2.4×10^{-4} ($\pm 4.8 \times 10^{-5}$) [h]	−25	5×10^3
P2b	$CHCl_3$	200/2	1.7×10^{-3} ($\pm 1.6 \times 10^{-4}$) [h]	−60	2×10^6
P3a	$CHCl_3$	150/2	6.6×10^{-3} ($\pm 2.0 \times 10^{-4}$) [h]	−10	5×10^4
P3b	$CHCl_3$	150/2	1.6×10^{-2} ($\pm 1.7 \times 10^{-3}$) [h]	−5	10^4
P(BTimR)-L	$CHCl_3$	300/2	1.1×10^{-2} ($\pm 9.8 \times 10^{-4}$) [e]	93	2×10^4
P(BTimR)-H	$CHCl_3$	270/2	3.8×10^{-2} ($\pm 2.1 \times 10^{-3}$) [e]	68	2×10^6
P3HT	$CHCl_3$	120/0.5	4×10^{-2} [h]	−14	10^3
P(BTimR)[a,b]	$CHCl_3$	240/2	1.1×10^{-2} [e]	75	2×10^7
P(BTimR-BT)[b]	DCB	180/0.5	8×10^{-3} [h]	−12	2×10^7

[a] Measured under vacuum. [b] Data taken from ref 60. [c] h and e indicate hole and electron mobility, respectively. Standard deviation values are shown in parentheses.

resulting in a higher HOMO energy. On the basis of eq 1, the calculated HOMO energies are −5.55, −5.45, −5.44, −5.40, and −5.38 eV for **P1**, **P2a**, **P2b**, **P3a**, and **P3b**, respectively. In comparison to **P3HT**, which has an oxidation potential onset of +0.33 V vs Fc/Fc^+ and a HOMO energy of −5.13 eV, measured under identical conditions, the HOMO energies of all BTI-based copolymers are substantially lower than that of **P3HT** by at least 0.25 eV. Thus, incorporating BTI as an electron-withdrawing unit into the polymer backbone should, all other things being equal, lead to materials with enhanced air stability vs **P3HT**.

Polymers **P1**, **P2a**, and **P2b** also exhibit two reversible reductive waves, which indicates that these materials can potentially function as n-type semiconductors. However, note that no detectable reductive waves are observed for polymer **P3**. For polymers **P1** and **P2** exhibiting reversible reductive waves, the LUMO energies are calculated from eq 2, whereas for polymer **P3** with no detectable reductive waves, the LUMO energies are estimated from the HOMO energy and the optical band gap using the eq 3. Relevant data are collected in Table 1. In comparison to the parent homopolymer **P(BTimR)**, which has a reduction potential onset of −1.33 eV,[60] **P1**, **P2a**, and **P2b** have reduction potential onsets (vs Fc/Fc^+) of −1.47, −1.58, and −1.54 V, respectively. The electrochemically derived LUMO energies are therefore −3.47, −3.33, −3.22, and −3.26 eV for **P(BTimTR)**, **P1**, **P2a**, and **P2b**, respectively. Therefore, incorporation of electron-donating units in the present materials leads to pronounced destabilization of the LUMO levels.

Polymer Thermal Properties. Thermal analysis of the BTI-based copolymers was carried out by differential scanning calorimetry (DSC) at a temperature ramp rate of 10 °C/min (Figure S24, Supporting Information). Two heating/cooling cycles were recorded for each sample to eliminate artifacts arising from residual solvent and/or H_2O. For polymers **P1**, **P2a,** and **P2b**, the DSC thermograms are featureless in the 25−340 °C temperature range, providing no evidence of mesophase transitions. However, polymers **P3a** and **P3b** exhibit clear thermal transitions during the heating/cooling cycles located at 287/272 °C for **P3a** and at 256/239 °C for **P3b**. Interestingly, the polymers functionalized with longer side chains exhibit lower transition temperatures. In essence, the side chains have already melted at temperatures approaching the transition temperatures and act as solvents, inducing the polymer backbones to melt at lower temperatures.[34]

Table 3. OFET Electrical Data for BG/TC Devices Fabricated from P3b Films Grown on HMDS-Treated Substrates and Annealed at the Indicated Temperatures (OFET data measured in ambient)

annealing temp. (°C)	μ ($cm^2\ V^{-1}\ s^{-1}$)[a]	V_t (V)	I_{on}/I_{off}
60	5.5×10^{-3} ($\pm 1.7 \times 10^{-4}$)	−23	7×10^4
120	1.4×10^{-2} ($\pm 4.6 \times 10^{-4}$)	−25	2×10^5
150	1.6×10^{-2} ($\pm 1.7 \times 10^{-3}$)	−5	10^4
200	1.5×10^{-2} ($\pm 8.1 \times 10^{-4}$)	−13	3×10^4
250	6.8×10^{-3} ($\pm 1.2 \times 10^{-3}$)	−36	2×10^4

[a] Standard deviations are shown in parentheses.

The development of mesophases in polymers **P3a** and **P3b** may be associated with the greater microstructural order, which should also lead to more efficient charge transport. The increasing of molecular weight of homopolymer leads to a more obvious endothermic transition at higher temperature for **P(BTimR)-H** (Figure S25, Supporting Information).

Field-Effect Transistor Fabrication and Device Characterization. Both bottom-gate/top-contact (BG/TC) and top-gate/bottom-contact (TG/BC) OFETs were fabricated to investigate the charge transport properties of the new BTI-based polymers. For the BG/TC devices, the semiconductor layer was deposited by spin coating a 5−10 mg/mL polymer solution (solvents used: 1,2-dichlorobenzene (DCB) for **P1**, chlorobenzene (CB) for **P2a**, and chloroform for **P2b**, **P3a**, and **P3b**) under ambient conditions on hexamethyldisilazane (HMDS)-treated, p-doped Si (001) wafers having a 300 nm thermally grown SiO_2 dielectric layer. The capacitance of the 300 nm SiO_2 gate insulator is ∼12 $nFcm^{-2}$. Prior to semiconductor deposition, the wafers were solvent cleaned by immersion in ethanol with sonication and then dried with a filtered stream of N_2, followed by 5 min plasma cleaning. Trimethylsilation of the Si/SiO_2 surface was carried out by exposing the silicon wafers to HMDS vapor at room temperature in a closed air-free container under N_2. After spin coating, the semiconductor films were annealed under N_2 or in vacuum at selected temperatures, as summarized in Tables 2 and 3.

OFET devices were completed by vapor deposition of the top gold electrodes through a shadow mask to define devices with channel lengths of 25−100 μm and widths of 500−2000 μm. Device characterization was typically performed under ambient

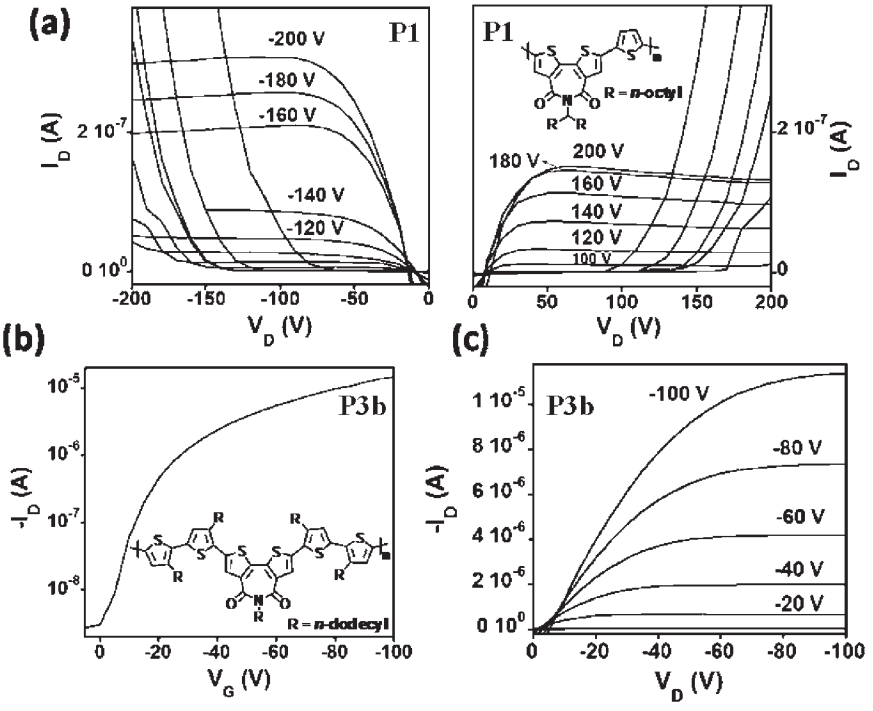

Figure 5. OFET response plots for **P1**- and **P3b**-based devices. (a) Output plots as a function of gate bias for **P1**-based devices measured under vacuum, (b) transfer plots (V_D = 100 V), and (c) output plots of **P3b**-based devices measured in ambient conditions.

conditions in a probe station as described in the Experimental Section (Supporting Information). Table 2 collects the average OFET performance for the present polymer series using optimized semiconductor film deposition conditions (at least five devices were measured for each sample), while Figure 5 shows selected output and transfer plots for polymer **P1** and **P3b** OFETs (see Table S1 in Supporting Information for additional data).

The present family of BTI-based copolymers and analysis of the OFET response provides valuable information on the effects of two different structural modifications in BTI systems: (i) sequential π-core expansion of the oligothiophene donor comonomer, affecting polymer electronic structure, and (ii) modification of the alkyl side chain length, which should affect film processability and crystallinity. The OFET trends summarized in Table 2 are in excellent agreement with the electrochemical measurements (Table 1). In fact, the HOMO energies extracted from the CV measurements increase in the order **P1** (−5.55 eV) < **P2** (−5.45 eV) < **P3** (−5.39 eV), while the hole field-effect mobilities follow exactly the same trend **P1** < **P2** < **P3**, specifically $\mu = 3.6 \times 10^{-4}$, 1.7×10^{-3}, and 1.6×10^{-2} cm^2 V^{-1} s^{-1} for **P1**, **P2b**, and **P3b**, respectively. These results indicate that by inserting electron-donating thiophene rings into the copolymer architecture, the HOMO energies approach the Fermi level of the gold electrodes (−5.0 eV), thus facilitating charge injection and increasing the field-effect hole mobility. The best performance for the present BG/TC devices is found for polymer **P3b**, which exhibits a field-effect mobility of 1.6×10^{-2} cm^2 V^{-1} s^{-1}, a threshold voltage of ∼−5 V, and a current on/off ratio of ∼10^4.

In the marked contrast to the above results, the LUMO levels are destabilized upon incorporating an increased number of thiophene subunits into the present polymers, thus rendering electron injection less favorable. Lacking any donor unit, homopolymer **P(BTimR)** exhibits n-type behavior with an electron mobility = 0.011 cm^2 V^{-1} s^{-1} under inert atmosphere.[60] However, copolymer **P1**, in which only a single thiophene ring is inserted into the repeat structure, is the only polymer in this class exhibiting ambipolar transport in vacuum, due to the relatively low-lying LUMO (−3.33 eV) compared to the other copolymers in this series having LUMOs from −3.22 to −3.26 eV. However, the **P1** LUMO is not sufficiently low-lying to enable electron transport in ambient;[51,52] thus, the ambipolar behavior of the **P1**-based OFETs is only observed in vacuum. This polymer exhibits very similar hole (3.6×10^{-4} cm^2 V^{-1} s^{-1}) and electron (4.6×10^{-4} cm^2 V^{-1} s^{-1}) mobilities in vacuum with I_{on}/I_{off} ratios ∼10^4 and thus has potential in complementary circuits.[68−70] P-type behavior is detected under ambient conditions with a hole mobility of ∼4.5×10^{-4} cm^2 V^{-1} s^{-1}. However, the threshold voltages measured for this polymer, for both electron and hole transport, are extremely large for practical applications, which may be due to the large formal energy barriers for efficient charge injection (1.67 eV for electron injection and 0.55 eV for hole injection) as well as trapping sites at the interface between the semiconductor and the SiO_2 dielectric substrate.[15]

We also investigated the device performance of homopolymer **P(BTimR)** for both M_n batches. The average electron mobility of **P(BTimR)-L** = 1.1×10^{-2} cm^2 V^{-1} s^{-1} for the optimized devices, comparable to our previous results. The high M_n batch **P(BTimR)-H** exhibits average electron mobility = 3.8×10^{-2} cm^2 V^{-1} s^{-1}, $I_{on}/I_{off} = 2 \times 10^6$, and a threshold voltage V_t = +68 V (Figure 6). Since both batches have identical optical and electrochemical properties, the significant difference in device performance must originate from the film morphology, which will be discussed in the following section.

Polymer Film Microstructures and Morphologies. In order to better understand the effects of the donor comonomer type and the various alkyl substituents on the electrical performance of the present BTI-based polymers, film microstructure and surface morphology were studied by specular X-ray diffraction (XRD)

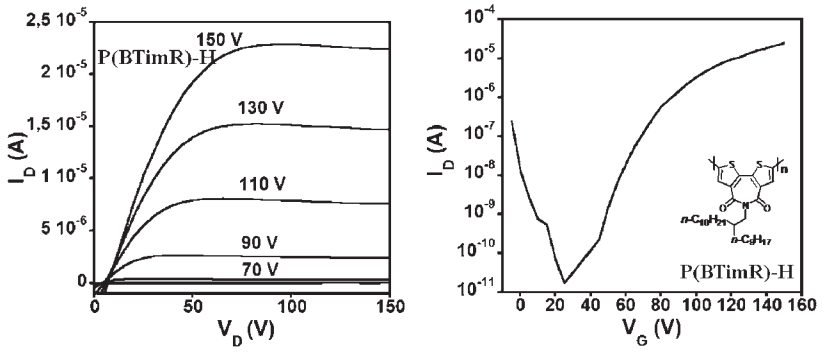

Figure 6. OFET response plots for the high molecular weight batch homopolymer **P(BTimR)-H** measured under vacuum. (Left) Output plots as a function of gate bias; (right) transfer plots (V_D = 150 V).

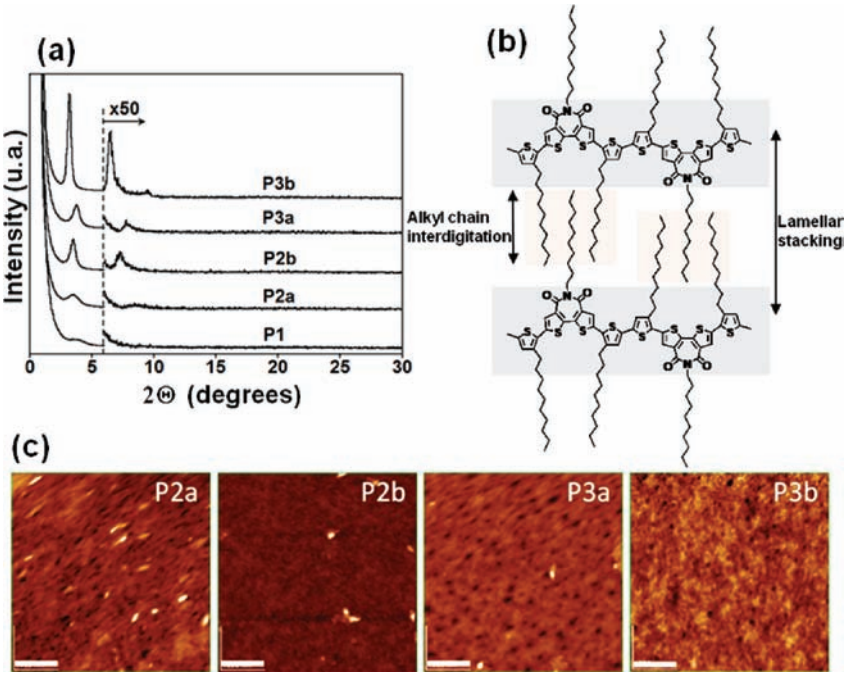

Figure 7. (a) Θ−2Θ X-ray diffraction scans of BTI-based polymer films spin cast onto hydrophobic HMDS-treated substrates, (b) cartoon showing suggested lamellar stacking for **P2a** in the polymer thin films, and (c) AFM images of thin films of the present polymers deposited on HMDS-treated Si/SiO_2 substrates and annealed at 150 (**P2a**, **P3a**, and **P3b**) and 200 °C (**P2b**). Scale bars correspond to 1 μm.

and tapping mode atomic force microscopy (AFM). Figure 7 shows Θ−2Θ XRD scans and AFM images for the present polymer films under the conditions yielding optimum BG/TC OFET performance. A single family of Bragg reflections is found for all the polymers. It is also seen that introducing thiophene rings into the main chain structure enhances thin film crystallinity,[71] presumably due to a more ordered $\pi-\pi$ stacking of the conjugated cores.[72]

From the Bragg reflections shown in Figure 7, the out-of-plane *d* spacings are estimated to be 23.9, 25.2, 25.2, 23.3, and 27.60 Å for polymers **P1**, **P2a**, **P2b**, **P3a**, and **P3b**, respectively. To better understand this trend, Figure 7b shows a sketch indicating the possible lamellar stacking of the polymers under study. From this diagram note that the backbone tilt angle should strongly depend on the substituent chain length and the extent of alkyl chain interdigitation. Interestingly, in the case of **P2a** and **P2b**, the *d* spacings are identical, while the data for **P2b** having a different substituent alkyl chain lengths indicate either a different tilt angle or a greater degree of alkyl group interdigitation. From the XRD data in Figure 7a, it is also clear that replacing *n*-decyl by *n*-dodecyl as the side chain enhances the film crystallinity in all cases, probably because of improved self-assembly driven by side chain crystallization,[33] which is also in agreement with the *d* spacings found for **P2a** and **P2b**. The greatest crystallinity is found for polymer **P3b**, with Bragg reflections up to third order. Furthermore, AFM images (Figure 7c) also indicate that the greatest crystallinity is for polymer **P3b**, films of which are characterized by better-defined grains. These results together with the highest HOMO energy are in accord with the greater OFET mobility for **P3b** versus the other BTI-based polymers.

For the most ordered, highest mobility polymer of this series **P3b**, we also investigated how film microstructure and BG/TC OFET performance evolve as a function of annealing at increasing temperatures. Figure 8 clearly shows that **P3b** crystallinity is enhanced when the annealing temperature is increased from 60 to 150 °C and then becomes less ordered as the annealing temperature

dx.doi.org/10.1021/ja107678m |*J. Am. Chem. Soc.* 2011, 133, 1405–1418

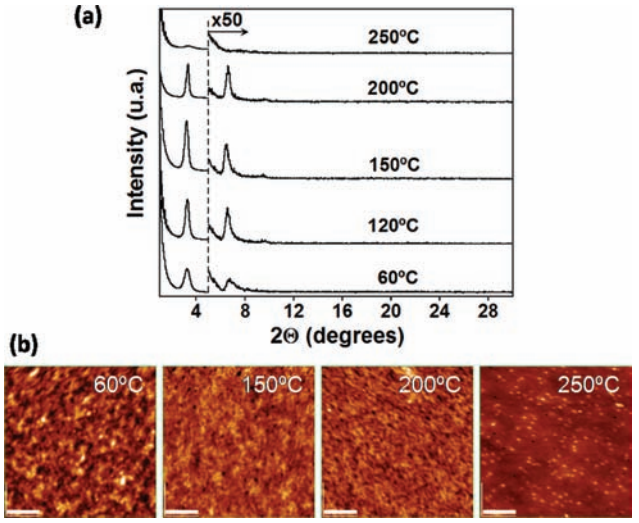

Figure 8. (a) Θ−2Θ X-ray diffraction scans and (b) AFM images of polymer **P3b** deposited on HMDS-treated Si/SiO_2 substrates and annealed at the indicated temperatures. AFM scale bars correspond to 1 μm.

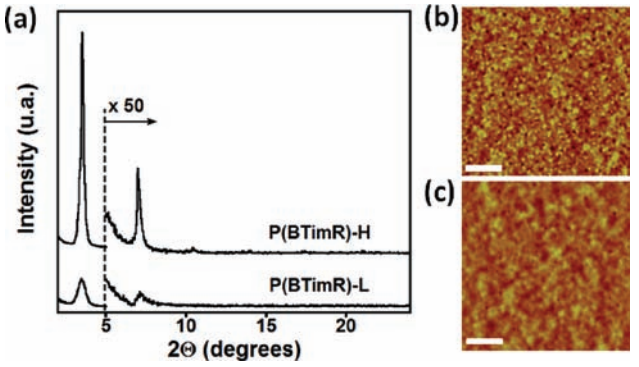

Figure 9. (a) Θ−2Θ X-ray diffraction scans of homopolymers **P(BTimR)-L** and **P(BTimR)-H** spin cast onto HMDS-treated substrates and annealed at 300 and 270 °C, respectively (temperatures yielding the highest electrical performance). (b) AFM image of a **P(BTimR)-H** film annealed at 270 °C, and (c) AFM image of a **P(BTimR)-L** film annealed at 300 °C. AFM scale bars = 1 μm.

is increased further. AFM images of the polymer films (Figure 8b) reveal similar evolution of morphologies for annealing temperatures ranging from 60 to 200 °C, which are characterized by the presence of small grains. In contrast, the AFM image of a film annealed at 250 °C shows no grains, in agreement with the lower crystallinity found in the XRD experiments (Figure 8a). Table 3 summarizes OFET performance for **P3b**-based devices as a function of the annealing temperature. Note that the OFET data mirror the XRD/AFM variations and microstructural trends. Thus, intermediate annealing temperatures (120−200 °C) result in optimum performance with $\mu > 10^{-2}$ $cm^2\ V^{-1}\ s^{-1}$, while lower performance is observed for **P3b** films annealed at both 60 and 250 °C. For **P(BTim-R)-H** homopolymer films, annealing at 270 °C yields optimum OFET response, in agreement with the morphology evolution indicated by XRD and AFM (Figure S26, Supporting Information).

In order to better understand the different device performances of the **P(BTimR)** homopolymers having different M_ns, Figure 9 compares the XRD spectra and AFM images for **P(BTimR)-L** and **P(BTimR)-H** thin films annealed at the temperatures that yield the highest electrical performance, 300 and 270 °C, respectively (see Supporting Information for the AFM images of the polymer films annealed at other temperatures). It is evident from both the XRD and the AFM data that the higher M_n batch polymer, **P(BTimR)-H**, yields far more crystalline films, exhibiting more intense XRD peaks and better-defined grains in the AFM images. This trend is in good agreement with electrical performance where the FET mobility is increased from 1.1×10^{-2} $cm^2\ V^{-1}\ s^{-1}$ for **P(BTimR)-L** to 3.8×10^{-2} $cm^2\ V^{-1}\ s^{-1}$ for **P(BTimR)-H**. These results clearly indicate the importance of controlling the molecular weight of these polymer semiconductors to achieve optimum device performance.[25,26]

Top-Gate/Bottom-Contact Transistors. The semiconducting properties of polymers **P(BTimR)-H**, **P3a,** and **P3b** were also characterized in top-gate/bottom-contact (TG/BC) OFET architectures. These devices were fabricated on glass substrates with gold source and drain electrodes (30 nm) deposited by thermal evaporation ($L = 50\ \mu$m, $W = 500\ \mu$m). The semiconductor films were deposited by spin coating 5 mg/mL DCB solutions and annealed in a vacuum oven at 110 °C. Either PMMA (poly(methylmethacrylate), capacitance =6.2 nF/cm^2) or Polyera ActivInk D2200 (polyolefin−polyacrylate, capacitance =5.4 nF/cm^2) was spin coated on top of the semiconductor films as the gate dielectric. Gold was then deposited by thermal evaporation as the gate electrode. Homopolymer **P(BTimR)-H**-based devices were evaluated under vacuum, and transfer plots were recorded at −150 V (V_D) and V_G from −10 to 150 V. Copolymer **P3a**- and **P3b**-based devices were evaluated under ambient, and transfer plots were recorded at −60 V (V_D) and V_G from 20 to −60 V. Transfer plots for **P(BTimR)-H**, **P3a**, and **P3b** using the two different gate dielectrics are presented in Figure 10, and extracted OFET data are summarized in Table 4.

The data collected in Table 4 clearly demonstrate the enhanced OFET performance of these TG/BC devices vs the BG/TC OFETs discussed earlier. **P(BTimR)-H**-based devices exhibit a maximum electron mobility = 0.19 $cm^2\ V^{-1}\ s^{-1}$ and $I_{on}/I_{off} = 10^5$ using D2000 as dielectric under vacuum. However, these OFETs no longer function when exposed to air due to the high polymer LUMO energies. **P3a**-based OFETs exhibit similar hole mobilities for both PMMA ($\mu \approx 0.061$ $cm^2\ V^{-1}\ s^{-1}$) and D2000 ($\mu \approx 0.068$ $cm^2\ V^{-1}\ s^{-1}$) dielectric materials and I_{on}/I_{off} ratios $\approx 10^5$. These mobilities are ∼10 times larger than those of the corresponding BG/TC OFETs. However, the enhancement in OFET performance for the **P3b**-based devices is not as significant, with average mobilities = 0.026 $cm^2\ V^{-1}\ s^{-1}$ using PMMA as the dielectric and 0.064 $cm^2\ V^{-1}\ s^{-1}$ using D2200 as the dielectric. The 3-fold lower mobility in **P3b**/PMMA devices versus **P3b**/D2200 devices can be explained by the poor film uniformity observable in the latter films under the optical microscope. The performance enhancement in TG/BC OFET devices has also been demonstrated for other polymeric semiconductors[14] and offers several advantages over the traditional bottom-gate/bottom-contact (BG/BT) OFET configuration: (i) lower contact resistance due to reduction of current crowding effects in staggered contact structures;[73] (ii) wider selection of gate dielectric materials to minimize charge trapping at the dielectric/semiconductor interfaces;[74] (iii) better device air stability afforded by encapsulation effects provided by the overlying gate dielectrics and gate electrodes;[74] (iv) favorable architecture for printed electronics in which every component can be applied by printing technology.[18]

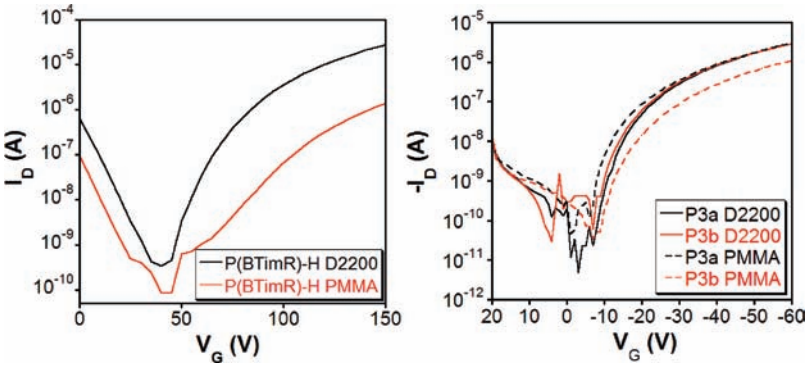

Figure 10. OFET transfer plots of current vs V_G for representative top-gate/bottom-contact **P(BTimR)-H**, **P3a**, and **P3b** devices with PMMA and D2200 as the indicated polymeric dielectrics.

Table 4. OFET Electrical Data for Polymers P(BTimR)-H, P3a, and P3b TG/BC Devices Using PMMA and ActivInk D2200 as the Gate Dielectrics

	PMMA dielectric			D2200 dielectric		
polymer	μ ($cm^2\ V^{-1}\ s^{-1}$)[a]	I_{on}/I_{off}	V_t (V)	μ ($cm^2\ V^{-1}\ s^{-1}$)[a]	I_{on}/I_{off}	V_t (V)
P(BTimR)-H	0.013 (0.017)	10^4	61	0.141 (0.189)	10^5	76
P3a	0.061 (0.067)	10^5	−18	0.068 (0.077)	10^5	−19
P3b	0.026 (0.031)	5×10^4	−21	0.064 (0.067)	10^5	−17

[a] Data in parentheses are the highest measured mobilities.

It is also instructive to compare the device performance of **P3** with that of **P3HT** in TG/BC structures. **P3HT** exhibits hole mobilities ≈ 0.02−0.1 $cm^2\ V^{-1}\ s^{-1}$ and $I_{on}/I_{off} = 10^2-10^3$ in TG/BC devices using Au/PMMA and Au/D2200 as contact/dielectric materials.[14] The hole mobilities of **P3a** and **P3b** are comparable to that of **P3HT** under the same conditions. However, the I_{on}/I_{off} ratio for devices fabricated from **P3HT** is ca. 2−3 orders of magnitude lower than that of devices fabricated from **P3**, which reflects the lower-lying **P3** HOMO.

Transistor Performance Stability. For n-type polymers, device air stability is mainly governed by electron affinities. Clearly, the BTI subunit is not sufficiently electron withdrawing to stabilize electron transport for both the n-type and the ambipolar polymers reported here. For semiconducting p-type polymers, OFET air stability is largely controlled by the ionization potentials.[75] Low ionization potentials usually result in oxidative doping by O_2, which erodes OFET performance by decreasing the I_{on}/I_{off} ratio due to increased off currents and threshold voltage shifts to positive values.[49,76] As seen in Figure 4 and Table 1, introduction of the BTI subunit in conjugated polymers increases the oxidation potentials of the copolymers as measured by cyclic voltammetry with respect to that of **P3HT** by at least 0.25 eV. This translates into lower-lying HOMO levels and consequently higher ionization potentials. This important characteristic makes the copolymers studied in this contribution far more resistant to O_2 doping than **P3HT**, which is demonstrated by analysis of OFET performance as a function of time.

Figure 11 shows transfer plots for **P3b**-based BG/TC OFETs measured immediately after device fabrication and after storage for 9 months under ambient conditions and also temporal evolution of **P3b**-based OFET ambient characteristics. From these plots, an identical field-effect mobility of 1.6×10^{-2} $cm^2\ V^{-1}\ s^{-1}$ and a threshold voltage of ∼−5 V are extracted for **P3b**-based devices after 2 months ambient exposure. The only difference is the I_{on}/I_{off} ratio, which slightly increases from 10^4 to 2×10^4 due to the decreased off current, which may originate from degradation of unintentionally p-doped polymer radical cations in air.[77,78] On storing the **P3b**-based FETs in ambient up to 9 months, the hole mobility is slightly decreased to 1.1×10^{-2} $cm^2\ V^{-1}\ s^{-1}$ with an identical I_{on}/I_{off} ratio and similar $V_t \approx -9$ V. These results underscore the impressive stability of **P3b** since in the case of air instability, a decreased I_{on}/I_{off} ratio is expected due to oxidative

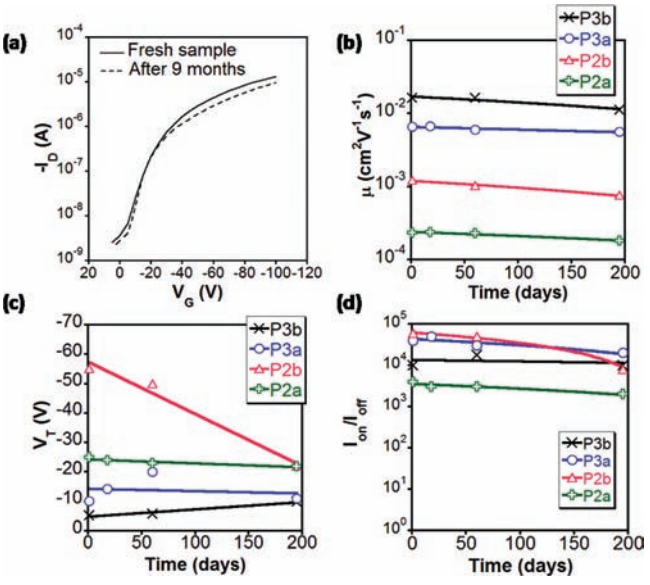

Figure 11. (a) Transfer plot (V_D = 100 V) for a fresh **P3b**-based device (solid line) and after 9 months storage in air (dashed line). Temporal evolution of OFET performance in air: (b) carrier mobility, (c) threshold voltage, and (d) I_{on}/I_{off} ratio for the present BTI-based polymers. Average values are shown.

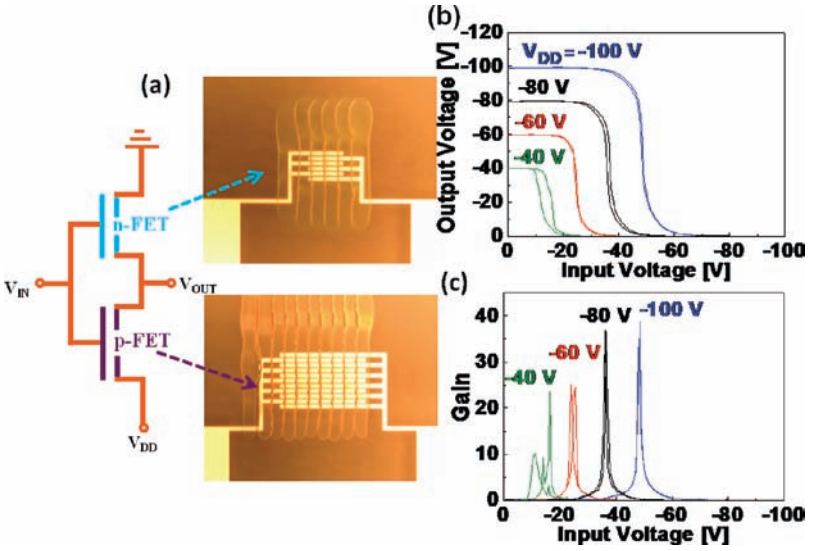

Figure 12. (a) Schematic layout of the complementary inverters fabricated from polymers **P3b** and **P(BTimR)-H** and optical image of the inkjet-printed devices, (b) static switching characteristics of an inverter, and (c) gains of the corresponding inkjet-printed inverter.

O_2 doping, which would increase the off current. Figure 11 also shows the temporal evolution of the OFET ambient characteristics for **P2a**-, **P2b**-, and **P3a**-based devices. All BG/TC devices fabricated from these materials are robust and air stable, with only slightly lower hole mobility, the same order I_{on}/I_{off} ratio, and similar V_t after 200 days storage. The only exception is those based on **P2b**, which exhibit a V_t shift of +30 V. The exact reason for the large V_t shift is unknown and cannot be only explained by its HOMO energy, since the most structurally similar polymer **P2a**-based devices exhibit essentially no V_t shift over the same storage period. For the present TG/BC devices, comparable air stabilities are again observed due to the low HOMO energies of these materials as well as the encapsulation effects of the TG/BC architecture.[74] In fact, field-effect mobilities remain basically constant over 60 days of air exposure. As an example, TG/BC **P3a**-based devices exhibit a field-effect mobility of ~0.06 cm^2 V^{-1} s^{-1}, a threshold voltage of ~−24 V, and an I_{on}/I_{off} ratio of ~10^5 when D2200 is used as the gate dielectric. When storage was extended to 9 months, the hole mobility (0.06 cm^2 V^{-1} s^{-1}) and threshold voltage (−24 V) also remain unchanged; however, the I_{on}/I_{off} ratio is decreased by 10× (see the transfer plots in Figure S28, Supporting Information).

Inkjet-Patterned Polymeric CMOS Inverters. Complementary inverters were fabricated by inkjet printing/patterning the present semiconducting polymers (see Supporting Information for detailed procedure). For monolithic integration of the p- and n-channel OFETs, **P3b** and **P(BTimR)-H** were chosen as the p-type and n-type semiconductors, since they show the highest hole and electron mobilities in this series, respectively. Their solutions were sequentially inkjet-printed onto photolithography patterned Au bottom-contact electrodes. The polymer gate dielectric PMMA was then spin coated on the conjugated polymers for a top-gated geometry. Figure 12 shows the voltage transfer characteristics (VTCs) of the resulting complementary inverter (p-channel, W/L = 5.0 mm/10 μm; n-channel, W/L = 1.0 mm/10 μm) at various supply voltages (V_{DD}). The static inverter characteristics show negligible bias hysteresis and high voltage gains (~ 40) at V_{DD} = −100 V; the voltage gain reported here is comparable to that of current state-of-the-art organic inverters.[14,69,70] The inverting voltage (V_{IN}) is slightly shifted in the positive direction with respect to 1/2 V_{DD} due to slightly different V_ts and charge carrier mobilities between the p- and the n-channel materials.

CONCLUSIONS

A new series of BTI-oligothiophene copolymers was synthesized and characterized. These systems contain electron-deficient BTI subunits and oligothiophenes having sequentially varied conjugation lengths as electron-rich cosubunits. The resulting copolymers exhibit similar band gaps (~1.80 eV); however, the energies of the frontier molecular levels (FMOs) vary based on the donor/acceptor interactions, which greatly affect OFET performance. As the conjugation length of donor blocks increases from monothiophene (**P1**) to bithiophene (**P2**) to tetrathiophene (**P3**), the p-type behavior becomes more pronounced and the holes become more mobile, resulting in greater hole mobilities. Compared to n-type homopolymer **P(BTimR)**, insertion of monothiophene subunits results in ambipolar **P1** with balanced hole and electron mobilities of ~10^{-4} cm^2 V^{-1} s^{-1}. Further increasing the oligothiophene donor conjugation length in **P2** and **P3** yields p-type response with hole mobilities of 10^{-3} and 10^{-2} cm^2 V^{-1} s^{-1}, respectively. We also investigated the influence of **P(BTimR)** homopolymer molecular weight on the film morphology and device performance. The high molecular weight batch, **P(BTimR)-H**, exhibits far greater performance than the low molecular weight one. Through device optimization using a TG/BC OFET architecture, **P(BTimR)-H** exhibits a high electron mobility of ~0.2 cm^2 V^{-1} s^{-1} in vacuum. Device optimization by employing TG/BC OFET architectures leads to hole mobilities approaching 0.1 cm^2 V^{-1} s^{-1} for **P3a** and **P3b**, comparable to that of **P3HT** devices fabricated under identical conditions. Furthermore, both the present BG/TC and TG/BC devices fabricated from **P3a** and **P3b** are remarkably air stable, and key OFET performance parameters (hole mobility, I_{on}/I_{off} ratio and V_t) exhibit negligible changes after storing the devices under ambient conditions for 200 m days. Finally, complementary inverters fabricated from **P3b** and **P(BTimR)-H** OFETs

achieve a high voltage gain of ~40. The present results demonstrate enhanced charge carrier mobility by optimizing polymer semiconductor molecular weight, tunability of charge carrier polarity, and achieving high hole mobility with good device air stability by adjusting frontier molecular orbital energies and optimizing film microstructures.

■ ASSOCIATED CONTENT

Supporting Information. Monomer/polymer synthesis and characterization; detailed procedure for fabrication and characterization of complementary inverters; ^{1}H and ^{13}C NMR spectra of all monomers; ^{1}H NMR spectra and DSC curves of all polymers; XRD and AFM images of polymer films; overlapped transfer plots of **P3a**-based TG/BC OFETs after different storage time; OFET device data for different deposition conditions of polymers. This material is available free of charge via the Internet at http://pubs.acs.org.

■ AUTHOR INFORMATION

Corresponding Author
a-facchetti@northwestern.edu; t-marks@northwestern.edu

■ ACKNOWLEDGMENT

We thank ONR (N00014-05-1-0766), AFOSR (FA9550-08-1-0331), and Polyera Corp. for support of this research and the NSF-MRSEC program through the Northwestern University Materials Research Science and Engineering Center for characterization facilities (DMR-0520513). The research leading to these results has also received funding from the European Community's Seventh Framework Programme under Grant Agreement 234808. Research fulfilled at Hanbat National University and ETRI was supported by Development of Next Generation RFID Technology for item-level applications (2008-F052-01) funded by the Ministry of Knowledge Economy (MKE) of Korea and Korea Basic Science Research Program through the National Research Foundation of Korea (NRF) funded by the Ministry of Education, Science and Technology (2010-0023180). We thank Dr. S. Lu of Polyera Corp. for GPC measurements.

■ REFERENCES

(1) Forrest, S. R. *Nature* **2004,** *428,* 911–918.
(2) Facchetti, A. *Mater. Today* **2007,** *10,* 28–37.
(3) Günes, S.; Neugebauer, H.; Sariciftci, N. S. *Chem. Rev.* **2007,** *107,* 1324–1338.
(4) Arias, A. C.; MacKenzie, J. D.; McCulloch, I.; Rivnay, J.; Salleo, A. *Chem. Rev.* **2010,** *110,* 3–24.
(5) Friend, R. H.; Gymer, R. W.; Holmes, A. B.; Burroughes, J. H.; Marks, R. N.; Taliani, C.; Bradley, D. D. C.; Dos Santos, D. A.; Brédas, J. L.; Logdlund, M.; Salaneck, W. R. *Nature* **1999,** *397,* 121–128.
(6) Lo, S. C.; Burn, P. L. *Chem. Rev.* **2007,** *107,* 1097–1116.
(7) Dimitrakopoulos, C. D.; Malenfant, P. R. L. *Adv. Mater.* **2002,** *14,* 99–117.
(8) Wen, Y.; Liu, Y. *Adv. Mater.* **2010,** *22,* 1331–1345.
(9) Cheng, Y.-J.; Yang, S.-H.; Hsu, C.-S. *Chem. Rev.* **2009,** *109,* 5868–5923.
(10) Thompson, B. C.; Fréchet, J. M. J. *Angew. Chem., Int. Ed.* **2008,** *47,* 58–77.
(11) Argun, A. A.; Aubert, P. H.; Thompson, B. C.; Schwendeman, I.; Gaupp, C. L.; Hwang, J.; Pinto, N. J.; Tanner, D. B.; MacDiarmid, A. G.; Reynolds, J. R. *Chem. Mater.* **2004,** *16,* 4401–4412.
(12) Beaujuge, P. M.; Reynolds, J. R. *Chem. Rev.* **2010,** *110,* 268–320.
(13) Hoth, C. N.; Choulis, S. A.; Schilinsky, P.; Brabéc, C. *J. Adv. Mater.* **2007,** *19,* 3973–3978.
(14) Yan, H.; Chen, Z.; Zheng, Y.; Newman, C.; Quinn, J. R.; Dotz, F.; Kastler, M.; Facchetti, A. *Nature* **2009,** *457,* 679–686.
(15) Zaumseil, J.; Sirringhaus, H. *Chem. Rev.* **2007,** *107,* 1296–1323.
(16) Sirringhaus, H.; Kawase, T.; Friend, R. H.; Shimoda, T.; Inbasekaran, M.; Wu, W.; Woo, E. P. *Science* **2000,** *290,* 2123–2126.
(17) McCulloch, I.; Heeney, M.; Chabinyc, M. L.; DeLongchamp, D.; Kline, R. J.; Coelle, M.; Duffy, W.; Fischer, D.; Gundlach, D.; Hamadani, B.; Hamilton, R.; Richter, L.; Salleo, A.; Shkunov, M.; Sporrowe, D.; Tierney, S.; Zhong, W. *Adv. Mater.* **2009,** *21,* 1091–1109.
(18) Allard, S.; Forster, M.; Souharce, B.; Thiem, H.; Scherf, U. *Angew. Chem., Int. Ed.* **2008,** *47,* 4070–4098.
(19) Murphy, A. R.; Fréchet, J. M. *J. Chem. Rev.* **2007,** *107,* 1066–1096.
(20) Anthony, J. E. *Chem. Rev.* **2006,** *106,* 5028–5048.
(21) Osaka, I.; McCullough, R. D. *Acc. Chem. Res.* **2008,** *41,* 1202–1214.
(22) Liu, S.; Wang, W.; Briseno, A. L.; Mannsfeld, S. C. B.; Bao, Z. *Adv. Mater.* **2009,** *21,* 1217–1232.
(23) Payne, M. M.; Parkin, S. R.; Anthony, J. E.; Kuo, C. C.; Jackson, T. N. *J. Am. Chem. Soc.* **2005,** *127,* 4986–4987.
(24) Anthony, J. E. *Angew. Chem., Int. Ed.* **2008,** *47,* 452–483.
(25) Kline, R. J.; McGehee, M. D.; Kadnikova, E. N.; Liu, J.; Fréchet, J. M. *J. Adv. Mater.* **2003,** *15,* 1519–1522.
(26) Kline, R. J.; McGehee, M. D.; Kadnikova, E. N.; Liu, J.; Fréchet, J. M. J.; Toney, M. F. *Macromolecules* **2005,** *38,* 3312–3319.
(27) Ahmed, E.; Kim, F. S.; Xin, H.; Jenekhe, S. A. *Macromolecules* **2009,** *42,* 8615–8618.
(28) McCullough, R. D.; Tristramnagle, S.; Williams, S. P.; Lowe, R. D.; Jayaraman, M. *J. Am. Chem. Soc.* **1993,** *115,* 4910–4911.
(29) McCullough, R. D.; Williams, S. P. *J. Am. Chem. Soc.* **1993,** *115,* 11608–11609.
(30) Bao, Z.; Dodabalapur, A.; Lovinger, A. J. *Appl. Phys. Lett.* **1996,** *69,* 4108–4110.
(31) Sirringhaus, H.; Tessler, N.; Friend, R. H. *Science* **1998,** *280,* 1741–1744.
(32) Cho, J. H.; Lee, J.; Xia, Y.; Kim, B.; He, Y.; Renn, M. J.; Lodge, T. P.; Frisbie, C. D. *Nat. Mater.* **2008,** *7,* 900–906.
(33) Sauve, G.; Javier, A. E.; Zhang, R.; Liu, J.; Sydlik, S. A.; Kowalewski, T.; McCullough, R. D. *J. Mater. Chem.* **2010,** *20,* 3195–3201.
(34) Osaka, I.; Zhang, R.; Sauve, G.; Smilgies, D. M.; Kowalewski, T.; McCullough, R. D. *J. Am. Chem. Soc.* **2009,** *131,* 2521–2529.
(35) Lim, E.; Jung, B. J.; Lee, J.; Shim, H. K.; Lee, J. I.; Yang, Y. S.; Do, L. M. *Macromolecules* **2005,** *38,* 4531–4535.
(36) Lu, G.; Usta, H.; Risko, C.; Wang, L.; Faccehtti, A.; Ratner, M. A.; Marks, T. J. *J. Am. Chem. Soc.* **2008,** *130,* 7670–7685.
(37) Zhang, M.; Tsao, H. N.; Pisula, W.; Yang, C.; Mishra, A. K.; Müllen, K. *J. Am. Chem. Soc.* **2007,** *129,* 3472–3473.
(38) McCulloch, I.; Heeney, M.; Bailey, C.; Genevicius, K.; MacDonald, I.; Shkunov, M.; Sparrowe, D.; Tierney, S.; Wagner, R.; Zhang, W.; Chabinyc, M. L.; Kline, R. J.; McGehee, M. D.; Toney, M. F. *Nat. Mater.* **2006,** *5,* 328–333.
(39) Ong, B. S.; Wu, Y.; Liu, P.; Gardner, S. *J. Am. Chem. Soc.* **2004,** *126,* 3378–3379.
(40) Liu, J.; Zhang, R.; Sauve, G.; Kowalewski, T.; McCullough, R. D. *J. Am. Chem. Soc.* **2008,** *130,* 13167–13176.
(41) Kim, D. H.; Lee, B.-L.; Moon, H.; Kang, H. M.; Jeong, E. J.; Park, J.-I.; Han, K.-M.; Lee, S.; Yoo, B. W.; Koo, B. W.; Kim, J. Y.; Lee, W. H.; Cho, K.; Becerril, H. A.; Bao, Z. *J. Am. Chem. Soc.* **2009,** *131,* 6124–6132.
(42) Guo, X.; Kim, F. S.; Jenekhe, S. A.; Watson, M. D. *J. Am. Chem. Soc.* **2009,** *131,* 7206–7207.
(43) Wang, Y.; Watson, M. D. *Macromolecules* **2008,** *41,* 8643–8647.
(44) Irvin, J. A.; Schwendeman, I.; Lee, Y.; Abboud, K. A.; Reynolds, J. R. *J. Polym. Sci., Part A: Polym. Chem.* **2001,** *39,* 2164–2178.
(45) Guo, X.; Watson, M. D. *Org. Lett.* **2008,** *10,* 5333–5336.

(46) Babel, A.; Jenekhe, S. A. *J. Am. Chem. Soc.* **2003,** *125,* 13656–13657.
(47) Tsao, H. N.; Cho, D.; Andreasen, J. W.; Rouhanipour, A.; Breiby, D. W.; Pisula, W.; Müllen, K. *Adv. Mater.* **2009,** *21,* 209–212.
(48) Murphy, A. R.; Liu, J.; Luscombe, C.; Kavulak, D.; Fréchet, J. M. J.; Kline, R. J.; McGehee, M. D. *Chem. Mater.* **2005,** *17,* 4892–4899.
(49) Meijer, E. J.; Detcheverry, C.; Baesjou, P. J.; van Veenendaal, E.; de Leeuw, D. M.; Klapwijk, T. M. *J. Appl. Phys.* **2003,** *93,* 4831–4835.
(50) Anthopoulos, T. D.; Anyfantis, G. C.; Papavassiliou, G. C.; de Leeuw, D. M. *Appl. Phys. Lett.* **2007,** *90,* 122105.
(51) Jones, B. A.; Facchetti, A.; Wasielewski, M. R.; Marks, T. J. *J. Am. Chem. Soc.* **2007,** *129,* 15259–15278.
(52) Usta, H.; Risko, C.; Wang, Z.; Huang, H.; Deliomeroglu, M. K.; Zhukhovitskiy, A.; Facchetti, A.; Marks, T. J. *J. Am. Chem. Soc.* **2009,** *131,* 5586–5608.
(53) de Leeuw, D. M.; Simenon, M. M. J.; Brown, A. R.; Einerhand, R. E. F. *Synth. Met.* **1997,** *87,* 53–59.
(54) Thompson, B. C.; Kim, Y. G.; McCarley, T. D.; Reynolds, J. R. *J. Am. Chem. Soc.* **2006,** *128,* 12714–12725.
(55) Gao, X.; Di, C.; Hu, Y.; Yang, X.; Fan, H.; Zhang, F.; Liu, Y.; Li, H.; Zhu, D. *J. Am. Chem. Soc.* **2010,** *132,* 3697–3699.
(56) Gsänger, M.; Oh, J.; Könemann, M.; Höffken, H.; Krause, A.-M.; Bao, Z.; Würthner, F. *Angew. Chem., Int. Ed.* **2010,** *49,* 740–743.
(57) Zhu, Y.; Champion, R. D.; Jenekhe, S. A. *Macromolecules* **2006,** *39,* 8712–8719.
(58) Crouch, D. J.; Skabara, P. J.; Lohr, J. E.; McDouall, J. J. W.; Heeney, M.; McCulloch, I.; Sparrowe, D.; Shkunov, M.; Coles, S. J.; Horton, P. N.; Hursthouse, M. B. *Chem. Mater.* **2005,** *17,* 6567–6578.
(59) McCulloch, I.; Bailey, C.; Giles, M.; Heeney, M.; Love, I.; Shkunov, M.; Sparrowe, D.; Tierney, S. *Chem. Mater.* **2005,** *17,* 1381–1385.
(60) Letizia, J. A.; Salata, M. R.; Tribout, C. M.; Facchetti, A.; Ratner, M. A.; Marks, T. J. *J. Am. Chem. Soc.* **2008,** *130,* 9679–9694.
(61) Fong, H. H.; Pozdin, V. A.; Amassian, A.; Malliaras, G. G.; Smilgies, D. M.; He, M.; Gasper, S.; Zhang, F.; Sorensen, M. *J. Am. Chem. Soc.* **2008,** *130,* 13202–13203.
(62) Osaka, I.; Abe, T.; Shinamura, S.; Miyazaki, E.; Takimiya, K. *J. Am. Chem. Soc.* **2010,** *132,* 5000–5001.
(63) Zagorska, M.; Krische, B. *Polymer* **1990,** *31,* 1379–1383.
(64) Koster, L. J. A.; Mihailetchi, V. D.; Blom, P. W. M. *Appl. Phys. Lett.* **2006,** *88,* 243502.
(65) Wu, P. -T.; Xin, H.; Kim, F. S.; Ren, G.; Jenekhe, S. A. *Macromolecules* **2009,** *42,* 8817–8826.
(66) Pommerehne, J.; Vestweber, H.; Guss, W.; Mahrt, R. F.; Bässler, H.; Porsch, M.; Daub, J. *Adv. Mater.* **1995,** *7,* 551–554.
(67) Meerholz, K.; Heinze, J. *Electrochim. Acta* **1996,** *41,* 1839–1854.
(68) Meijer, E. J.; de Leeuw, D. M.; Setayesh, S.; van Veenendaal, E.; Huisman, B. H.; Blom, P. W. M.; Hummelen, J. C.; Scherf, U.; Kadam, J.; Klapwijk, T. M. *Nat. Mater.* **2003,** *2,* 834–834.
(69) Bijleveld, J. C.; Zoombelt, A. P.; Mathijssen, S. G. J.; Wienk, M. M.; Turbiez, M.; de Leeuw, D. M.; Janssen, R. A. J. *J. Am. Chem. Soc.* **2009,** *131,* 16616–16617.
(70) Kim, F. S.; Guo, X.; Watson, M. D.; Jenekhe, S. A. *Adv. Mater.* **2010,** *22,* 478–482.
(71) Durban, M. M.; Kazarinoff, P. D.; Luscombe, C. K. *Macromolecules* **2010,** *43,* 6348–6352.
(72) Osaka, I.; Zhang, R.; Liu, J.; Smilgies, D.-M.; Kowalewski, T.; McCullough, R. D. *Chem. Mater.* **2010,** *22,* 4191–4196.
(73) Street, R. A.; Salleo, A. *Appl. Phys. Lett.* **2002,** *81,* 2887–2889.
(74) Chen, Z.; Lemke, H.; Albert-Seifried, S.; Caironi, M.; Nielsen, M. M.; Heeney, M.; Zhang, W.; McCulloch, I.; Sirringhaus, H. *Adv. Mater.* **2010,** *22,* 2371–2375.
(75) Zhang, W.; Smith, J.; Watkins, S. E.; Gysel, R.; McGehee, M.; Salleo, A.; Kirkpatrick, J.; Ashraf, S.; Anthopoulos, T.; Heeney, M.; McCulloch, I. *J. Am. Chem. Soc.* **2010,** *132,* 11437–11439.
(76) Bao, Z.; Lovinger, A. J.; Dodabalapur, A. *Appl. Phys. Lett.* **1996,** *69,* 3066–3068.
(77) Oh, J. H.; Liu, S.; Bao, Z.; Schmidt, R.; Würthner, F. *Appl. Phys. Lett.* **2007,** *91,* 212107.
(78) Schmidt, R.; Oh, J. H.; Sun, Y.; Deppisch, M.; Krause, A. M.; Radacki, K.; Braunschweig, H.; Konemann, M.; Erk, P.; Bao, Z.; Würthner, F. *J. Am. Chem. Soc.* **2009,** *131,* 6215–6228.